



Article

Polarization Splitting at Visible Wavelengths with the Rutile TiO₂ Ridge Waveguide

Xinzhi Zheng^{1,2}, Yujie Ma^{1,*} , Chenxi Zhao^{1,2}, Bingxi Xiang³ , Mingyang Yu¹, Yanmeng Dai¹, Fang Xu¹, Jinman Lv¹, Fei Lu⁴, Cangtao Zhou¹ and Shuangchen Ruan^{1,*}

¹ Shenzhen Key Laboratory of Ultraintense Laser and Advanced Material Technology, Center for Advanced Material Diagnostic Technology, College of Engineering Physics, Shenzhen Technology University, Shenzhen 518118, China; 2110416034@stumail.sztu.edu.cn (X.Z.); 2200413002@stumail.sztu.edu.cn (C.Z.); yumingyang@sztu.edu.cn (M.Y.); daiyanmeng@sztu.edu.cn (Y.D.); xufang@sztu.edu.cn (F.X.); lvjinman@sztu.edu.cn (J.L.); zcangtao@sztu.edu.cn (C.Z.)

² College of Application and Technology, Shenzhen University, Shenzhen 518118, China

³ College of New Materials and New Energies, Shenzhen Technology University, Shenzhen 518118, China; xiangbingxi@sztu.edu.cn

⁴ School of Information Science and Engineering, Shandong University, Jinan 250100, China; lufei@sdu.edu.cn

* Correspondence: mayujie@sztu.edu.cn (Y.M.); scruan@sztu.edu.cn (S.R.)

Abstract: On-chip polarization control is in high demand for novel integrated photonic applications such as polarization division multiplexing and quantum communications. However, due to the sensitive scaling of the device dimension with wavelength and the visible-light absorption properties, traditional passive silicon photonic devices with asymmetric waveguide structures cannot achieve polarization control at visible wavelengths. In this paper, a new polarization-splitting mechanism based on energy distributions of the fundamental polarized modes in the r-TiO₂ ridge waveguide is investigated. The bending loss for different bending radii and the optical coupling properties of the fundamental modes in different r-TiO₂ ridge waveguide configurations are analyzed. In particular, a polarization splitter with a high extinction ratio operating at visible wavelengths based on directional couplers (DCs) in the r-TiO₂ ridge waveguide is proposed. Polarization-selective filters based on micro-ring resonators (MRRs) with resonances of only TE or TM polarizations are designed and operated. Our results show that polarization-splitters for visible wavelengths with a high extinction ratio in DC or MRR configurations can be achieved with a simple r-TiO₂ ridge waveguide structure.

Keywords: on-chip polarization splitting; r-TiO₂ thin film; optical ridge waveguide; micro-ring resonator



Citation: Zheng, X.; Ma, Y.; Zhao, C.; Xiang, B.; Yu, M.; Dai, Y.; Xu, F.; Lv, J.; Lu, F.; Zhou, C.; et al. Polarization Splitting at Visible Wavelengths with the Rutile TiO₂ Ridge Waveguide.

Nanomaterials **2023**, *13*, 1891. <https://doi.org/10.3390/nano13121891>

Academic Editor: Nam-Hoon Kim

Received: 22 May 2023

Revised: 16 June 2023

Accepted: 18 June 2023

Published: 20 June 2023



Copyright: © 2023 by the authors. Licensee MDPI, Basel, Switzerland. This article is an open access article distributed under the terms and conditions of the Creative Commons Attribution (CC BY) license (<https://creativecommons.org/licenses/by/4.0/>).

1. Introduction

On-chip polarization handling devices play important roles in many applications, including polarization diversity/(de)multiplexing for realizing polarization-transparent photonic integrated circuits (PICs) [1–3], polarization division multiplexing (PDM) [4,5], coherent optical communications [6–9], and quantum photonics integrated circuits [10]. Silicon nanophotonic waveguides with ultrahigh-index contrast can achieve birefringence as high as 0.7 of two fundamental modes [11,12], making possible fabrication of ultra-compact on-chip polarization handling devices (OCPHDs) [9]. Novel silicon-on-insulator (SOI) OCPHDs, but only for the infrared (IR) regime, have been proposed [9–12]. However, modern quantum PIC applications often require polarization manipulation at visible wavelengths [13,14]. Integrated photonic platforms operating at visible wavelengths are of great interest for applications ranging from quantum optics and metrology to bio-sensing and biomedicine [15–17]. Furthermore, visible wavelength light is used for quantum state preparation [18], manipulation [19], readout of color centers [20], quantum dots [21], and various quantum emitters in 2D materials [22,23]. These applications will inevitably involve polarization-sensitive devices, so it is necessary to develop on-chip PBSs for visible

wavelengths. For example, visible light polarization control on-chip can be applied in quantum systems and underwater datacom for advanced cooling schemes for quantum computing [24].

The polarization beam splitter (PBS) is regularly used for separating/combining TE and TM mode polarizations. Most existing PBSs work in the near-infrared regime and require rather demanding fabrication. Various structures have been proposed to realize on-chip PBSs [11,25–41], such as those in multimode interferometers [25,26], the Mach–Zehnder interferometer (MZI) [27–31], photonic crystals (PhC) [32–35], mode evolutions [36], arrayed-waveguide gratings (AWGs) [37], and the plasmonic waveguide [38]. Compared with such structures, directional couplers (DCs) and asymmetric direct couplers (ADCs) for PBSs are more convenient due to their structural and design simplicity [11,39–41]. The performance of DCs and ADCs relies on the distinct birefringence of two fundamental modes in silicon waveguides resulting from the geometrical asymmetry in the sub-micrometer cross-section. However, because of the visible-light absorbing properties of silicon, as well as the dimension-scaling requirements of silicon nanowires, SOI PBS operating at visible wavelengths is still unavailable. Transparent materials, such as lithium niobite (LN) and titanium dioxide (TiO_2), have relatively low refractive index compared with silicon, but it is difficult to separate the fundamental modes' polarizations using birefringence by adjusting the geometrical asymmetry for the visible wavelengths. Accordingly, a polarization-control device with a simple waveguide structure for visible wavelengths is desirable.

Titanium dioxide (TiO_2) is promising for realizing visible-spectrum integrated photonic devices due to its favorable optical properties such as relatively high refractive index, large bandgap, low thermal expansion coefficient, negative thermo-optic coefficient [42–44], and large Kerr nonlinearity [45,46]. Moreover, bio-compatibility and environmental friendliness allow its wide use [47]. Among its three (anatase, rutile, and brookite) phases, TiO_2 in the rutile phase (r- TiO_2) has the largest (>2.7) refractive index as well as the best thermal stability. Recently, we successfully fabricated a heterostructure composed of an r- TiO_2 thin film on a SiO_2 substrate through ion implantation combined with Cu-Sn bonding [48], thereby opening a door for achieving on-chip polarization-handling devices for the visible spectrum. However, in order to realize optical waveguides on r- TiO_2 thin films using micromachining techniques, it is first necessary to estimate the workable and optimum structural parameters of the waveguide.

We propose here a novel polarization-splitting mechanism based on a simple ridge waveguide structure that is applicable to visible light. The characteristics of bending loss with different bending radii and optical coupling properties for the fundamental polarization modes in certain selected r- TiO_2 ridge waveguide configurations, as well as the polarization-splitting mechanism involving different energy distributions of the TE₀ and TM₀ modes in the ridge waveguide, are analyzed. A polarization-splitter with a high extinction ratio operating for visible wavelengths based on DCs in the r- TiO_2 ridge waveguide structure, with a transmission extinction ratio of −40 dB for the TE/TM polarization beam splitter, is used. We also propose an MRR-based polarization-selective filter in the r- TiO_2 ridge waveguide structure. For the TM MRR, the transmission of the TE₀ polarization mode at the drop port is reduced to −58 dB. For the TE MRR, the transmission of the TM polarization mode at the drop port is reduced to −40 dB. Our results suggest that a polarization splitter with a high extinction ratio for the visible wavelengths in DC or MRR configurations can be achieved by tailoring the structural dimension of the r- TiO_2 ridge waveguide.

2. Materials and Methods

The ridge waveguide is widely used in various integrated optical devices [49]. As shown in Figure 1a, it consists of a slab with a superimposed strip, where H and h are the rib and slab heights, respectively, and W is the rib width. According to the simulation results for optical transmission in the r- TiO_2 ridge waveguide based on the 3D-FDTD model, we found that the optical energy distribution of the two fundamental modes (TE₀

and TM₀) in the r-TiO₂ ridge waveguide structure is distinct. As shown in Figure 1a,b, more TE₀ energy tends to propagate in the lower slab layer, and most TM₀ energy tends to be in the rib strip. Due to these energy distribution properties, if the waveguide is bent, the TE₀ mode tends to leak from the lower layer, and it is easily coupled to the waveguides adjacent to the latter, as shown in Figure 1c,d. The difference in the energy distributions of the TE₀ and TM₀ modes can thus be used for the polarization separation of light. Moreover, this polarization-splitting mechanism is applicable to the visible spectrum, suggesting its use in on-chip polarization-handling devices for visible wavelengths.

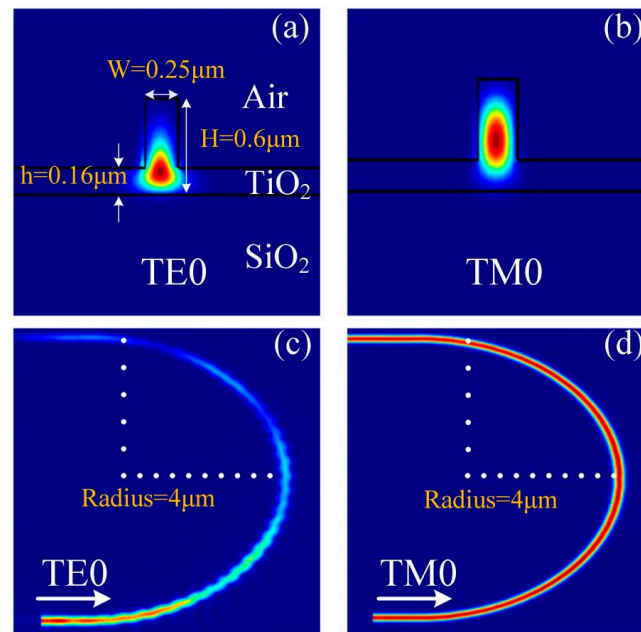


Figure 1. Energy distribution (arbitrary units; red: strongest, blue: weakest) in a ridge waveguide for the TE₀ (a) and TM₀ (b) modes at 635 nm. Energy distribution of the fundamental polarized modes propagating in a bent rib waveguide with the cross-section shown in (a) for the TE₀ (c) and TM₀ (d) modes, respectively. The radius of the bent waveguide is 4 μm.

In order to effectively separate the TE₀ and TM₀ modes for optimizing polarization-splitting performance, the width and thickness of the r-TiO₂ ridge waveguide structure should be tailored. To distinguish the two fundamental modes, their distribution difference should be enhanced. Accordingly, h/H should be as small as possible in order to inhibit TM₀ mode propagation in the lower slab, and W/H should be as small as possible in order to inhibit TE₀ mode propagation in the top rib strip. Moreover, to prevent interference by the higher-order modes, the ridge waveguide should be restricted to single-mode propagation, i.e., h/H should not be too small. A too-small h/H would lead to the waveguide height increasing, so higher-order mode interactions can occur. Meanwhile, a too-small W/H would make it difficult for light to propagate in the waveguide. Therefore, there should be a threshold value for both h/H and W/H to guarantee single-mode propagation in the r-TiO₂ ridge waveguide, and the r-TiO₂ ridge waveguide structural parameters should be appropriately tailored. In order to maintain low-loss, single-mode transmission and retain the TE₀ mode in the lower slab layer as much as possible, we found that for $W = 0.25 \mu\text{m}$ rib width and $0.6 \mu\text{m}$ r-TiO₂ film thickness, the minimum value of h should be $0.16 \mu\text{m}$.

The mode energy distribution of the r-TiO₂ ridge waveguide, obtained using the finite difference eigenmode (FDE) code [50], which is based on solving Maxwell's equations for a cross-sectional mesh in the waveguide, is shown in Figure 1a,b, where the effective refractive indices used are $n(\text{TiO}_2) = 2.72$ (core), $n(\text{SiO}_2) = 1.444$ (substrate), and $n(\text{air}) = 1$ (cladding). To calculate the bending loss of polarized light in the curved r-TiO₂ waveguide,

the model conducted using FDTD solutions from Lumerical software and the 3D-FDTD algorithm were used for simulation, and the detailed calculation mechanism is shown in Refs. [51,52]. The light source in Figure 1c,d is the fundamental TE₀ mode and fundamental TM₀ mode, respectively. The mesh accuracy is 20 nm, and all boundary conditions are set to be PML conditions. There are mainly three types of propagation loss in the r-TiO₂ waveguide, which are scattering loss, absorption loss, and bending loss. The absorption loss can be negligible in the simulation model, and the bending loss that depends on the waveguide structure, especially the radius of the curved waveguide, is discussed in the following section. The scattering loss attributed to the scattering of propagating light from the rough side wall of the waveguide can be simulated by setting the meshing, and the scattering loss occurs when the simulation meshing is 20 nm. According to the experimental results in Ref. [53], the propagation loss in the strip waveguide with a width of 250 nm and a height of 70 nm on the amorphous TiO₂ thin film was determined to be 7.5 dB/cm. In comparison, the propagation loss calculated to be around 1.1 dB/cm in the r-TiO₂ ridge waveguide proposed in this paper is reasonable. Electron beam lithography (EBL) and inductively coupled plasma etching (ICP) were used to fabricate the ridge waveguide structure on the r-TiO₂ thin film, and the fabrication process is briefly demonstrated here. Firstly, chromium and photoresist thin films are deposited on the sample surface successively, and the waveguide pattern is exposed and developed on the photoresist. Then, the pattern of the photoresist is transferred to the r-TiO₂ thin film using ICP etching technology, and finally, the etching effect is observed using a scanning electron microscope (SEM).

As shown in Figure 2a,b, the bending loss in the TE₀ and TM₀ modes decreases with an increasing radius of the curved waveguide. In the curved r-TiO₂ ridge waveguide, the bending loss in the TE₀ mode is clearly larger than that in the TM₀ mode, especially when the radius is above 4 μm. The bending loss in the TM₀ mode decreases dramatically as the bending radius increases from 2 μm to 4 μm, but gradually decreases with a further radius increase. When the radius is 4 μm, the bending loss in the TM₀ mode is around 0.007 dB/μm, but that in the TE₀ mode is about 1.43 dB/μm. Thus, the TM₀ mode can propagate in this curved r-TiO₂ waveguide with a radius of 4 μm with very low bending loss, but very little TE₀ mode energy is retained due to its large bending loss when transmitting through the bending structure. That is, the two fundamental modes can be well separated using a bending r-TiO₂ waveguide with an appropriate radius. Furthermore, Figure 2c,d shows that varying the rib width *W* and slab height *h* has a negligible effect on the bending loss. In particular, the bending loss remains almost the same for the TM₀ mode, and that in the TE₀ mode is also limited. In fact, the size of a bending waveguide can be increased without affecting the bending loss. Accordingly, a curved r-TiO₂ waveguide structure, such as the MRR, can be designed to separate the TE₀ and TM₀ modes since the TE₀ mode tends to leak from the lower slab layer.

The difference in the coupling efficiencies of the TE₀ and TM₀ modes in r-TiO₂ ridge waveguides was also investigated. The coupling coefficient was obtained using the Lumerical 3D-FDTD simulation code, which is based on the 3-dimensional solution of the Maxwell equations. Figure 3a,b shows that the TE₀ and TM₀ modes in the two adjacent r-TiO₂ waveguides are coupled, but they are out of phase. The energy in the TE₀ mode is of the period $L_{TE} = 15 \mu\text{m}$, and that in the TM₀ mode is $L_{TM} = 60 \mu\text{m}$. Therefore, the coupling times of the two fundamental modes in the two adjacent waveguides can be modulated by changing the coupling length(s) of the waveguides. For example, Figure 3a,b shows that if the coupling length is 60 μm and the coupling distance is 0.2 μm, the TM₀ mode will be coupled from waveguide 1 to waveguide 2, and the TE₀ mode will be coupled from waveguide 1 to waveguide 2 twice: eventually back to waveguide 1, i.e., “over-coupling” occurs. Therefore, the two fundamental modes can be separated into different waveguides by tailoring the coupling parameters. Figure 3c,d shows the corresponding transmission spectra of the TE₀ and TM₀ modes in the two adjacent r-TiO₂ waveguides, respectively. Moreover, the coupling periods of the TE₀ and TM₀ modes increase with the coupling distance. From these results, we can see that the coupling length and distance in the

two adjacent r-TiO₂ waveguides can be controlled in order to selectively separate the two fundamental modes.

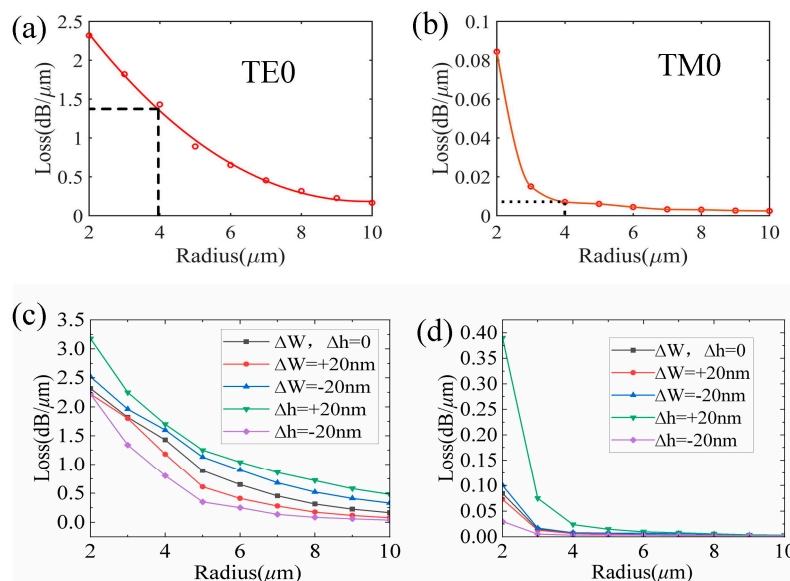


Figure 2. The bending loss in a 635 nm curved ridge waveguide for the TE₀ mode (a) and TM₀ mode (b) with different radii, and that for the TE₀ mode (c) and TM₀ mode (d) versus the waveguide width ΔW and slab height Δh .

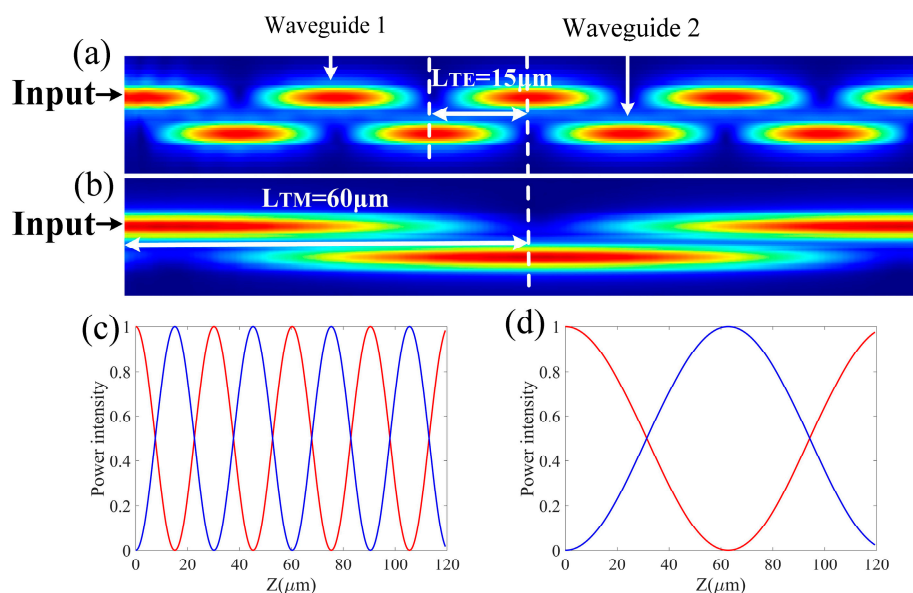


Figure 3. The electric fields of the TE₀ (a) and TM₀ (b) modes along the coupling length in the upper and lower waveguides, and the corresponding field intensities of the (c) TE₀ and (d) TM₀ modes in the upper (red curve) and lower (blue curve) waveguides. One can see that for both modes, the fields in the two adjacent waveguides are exactly out of phase, and there is no wave attenuation.

3. Results and Discussion

The PBS is one of the most important polarization-handling devices for separating/combining TE and TM polarizations. Here, a PBS based on the DC mechanism that can be operated in the visible spectrum is proposed. This PBS, consisting of a TM polarization beam splitter and a TE polarization beam splitter in the r-TiO₂ ridge waveguide, is designed according to the analysis above and shown in Figure 4. Light enters the main (straight) waveguide through the input port, and the TM₀ and TE₀ modes are separated and coupled

to the polarization beam splitters. The TM polarization beam splitter consists of a curved waveguide connected to two straight waveguides, and its width is $W1 = 0.25 \mu\text{m}$. According to the above analysis, in order to separate two fundamental modes as much as possible, the coupling length $L1$ and the coupling gap1 between the TM polarization beam splitter and the main straight waveguide are $60 \mu\text{m}$ and $0.2 \mu\text{m}$, respectively. Most of the TM₀ mode will then be coupled to the TM polarization beam splitter. The TE₀ mode is excluded from the latter due to over-coupling, as discussed. Instead, it propagates along the main straight waveguide and is eventually coupled to the TE polarization beam splitter. In the TM polarization beam splitter, a curved waveguide structure with bending radius $R1 = 4 \mu\text{m}$ is used to further remove the TE₀ mode, which suffers high bending loss ($1.43 \text{ dB}/\mu\text{m}$). The bending loss in the TM₀ mode in the curved waveguide is only $0.007 \text{ dB}/\mu\text{m}$, so that the TM₀ mode can propagate through the curved waveguide with little loss and exit from the Cross port. For the TE polarization beam splitter, two parallel coupled straight waveguides with different lengths are used to couple to the main waveguide. The coupling gap2 is $0.3 \mu\text{m}$, and the coupling length $L2$ is $\approx 30 \mu\text{m}$. With these coupling parameters, the TE₀ mode propagating along the main waveguide will be coupled to waveguide 1, and then to waveguide 2, and be detected at the Through port. This TE polarization beam splitter with three parallel straight waveguides can effectively inhibit the TM₀ mode from being coupled to the straight waveguide 2 because of its weak coupling efficiency.

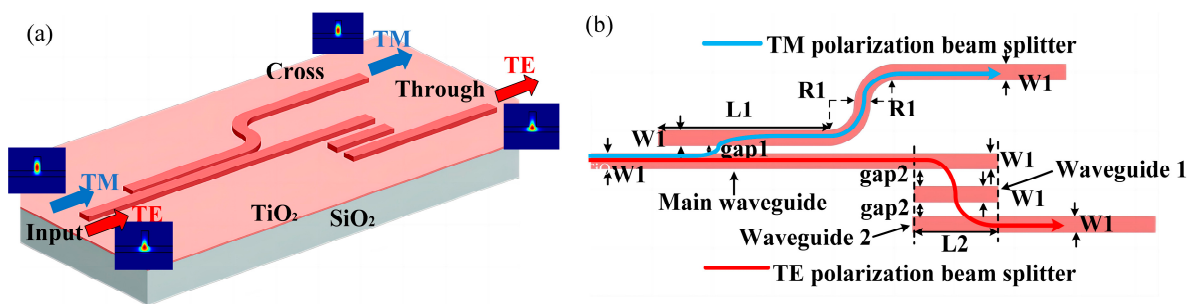


Figure 4. Schematic showing the proposed PBS (a) and its top view (b).

The transmission of the TE₀ mode and TM₀ mode energy in the proposed r-TiO₂ PBS were numerically simulated, and the results are shown in Figure 5a,b. In the TM polarization beam splitter shown in Figure 5a, the TM₀ mode is coupled from the main straight waveguide to the TM polarization beam splitter and propagates along the waveguide with low loss. In contrast, the TE₀ mode is coupled between the main and adjacent straight waveguides of the TM polarization beam splitter four times and then back to the main straight waveguide. It is then coupled to the TE polarization beam splitter, and output from the Through port. The transmitted spectrum at the Cross and Through ports are shown in Figure 5c,d, respectively. We see that for 610 to 660 nm light, the largest polarization extinction ratio for both the TM and TE beam splitters in our PBS reaches almost -40 dB , and polarization splitting of the TE beam splitter is more stable than that of the TM beam splitter. The polarization extinction ratio of the TE₀ and TM₀ modes in the TM polarization beam splitter can be enhanced by increasing the length of the curved waveguide. Thus, polarization separation with a high extinction ratio for the visible spectrum can be achieved with the r-TiO₂ ridge waveguide PBS.

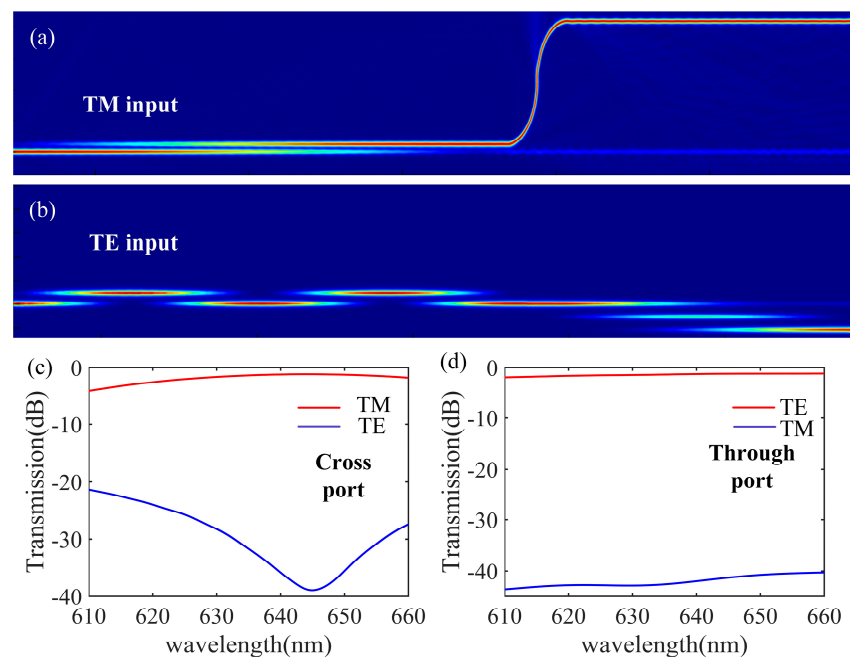


Figure 5. Optical field distribution of the r-TiO₂ ridge waveguide PBS for the TM (a) and TE (b) modes. Calculated optical transmission of the Cross (c) and Through (d) ports for the TM and TE polarizations.

The micro-ring resonator (MRR) is a basic component of optical platforms [54,55]. Because of its ultrahigh quality factor and small mode volume, MRR is useful in integrated and optical devices as well as information processing technologies, including wavelength division multiplexing (WDM) and polarization division multiplexing (PDM). Here we present a polarization-selective filter based on an add–drop type MRR in the r-TiO₂ ridge waveguide structure. The add–drop type MRR consists of a micro-ring waveguide coupled to two access waveguides with four ports, namely the Input, Through, Add, and Drop ports. For an MRR with bending radius R , the circumference of the micro-ring waveguide is $l = 2\pi R$, and the resonance wavelength is $\lambda = n_{eff}l/m$. Assuming that the coupling regions on both sides of the micro-ring are the same, i.e., $t_1 = t_2 = t$ and $k_1 = k_2 = k$, where k_1 (k_2) is the coupling coefficient and t_1 (t_2) the transmittance coefficient in the coupling region consisting of the input and the micro-ring waveguides (the output and the micro-ring waveguides), the peak power T_{drop} of the transmission is

$$T_{drop} = \frac{k^4 \alpha}{(1 - \alpha t^2)^2} \quad (1)$$

so that the peak power T_{drop} approaches zero for

$$k^2 \alpha^{1/2} \ll 1 \quad (2)$$

Therefore, in order to achieve MRR-based, polarization-selective optical filters, one can manipulate the polarization-dependent bending loss and coupling ratio of the MRRs by tailoring the waveguide structure. Resonance in the undesired polarization mode in the ring can be suppressed by minimizing its evanescent coupling and/or enhancing its bending loss. For the desired polarization mode, the coupling ratio and the bending loss should be optimized to satisfy the low loss and high extinction ratio. That is, a polarization beam splitter with an ultra-high extinction ratio can be achieved by controlling the structural parameters of the r-TiO₂ MRR. Based on the above numerical analysis, an r-TiO₂ MRR-based, TM-polarization-selective optical filter is proposed. An r-TiO₂ MRR in a ridge waveguide with radius $R = 4 \mu\text{m}$ can result in a bending loss of $0.007 \text{ dB}/\mu\text{m}$ for the TM₀

mode and 1.43 dB/ μm for the TE₀ mode for 635 nm light transmission around the ring. That is, the TM₀ mode can propagate with low bending loss, and the TE₀ mode decays, in the micro-ring waveguide. In order to achieve an ultra-high polarization extinction ratio, the coupling coefficient of the TE₀ and TM₀ modes between the straight and the ring waveguides should be precisely adjusted. Accordingly, the coupling strengths of the TE₀ and TM₀ modes for different coupling lengths were calculated, and the results are shown in Figure 6c. Based on these simulation results, a racetrack resonator, as shown in Figure 6a, was designed. The coupling length is 40 μm and the coupling distance gap₁ is 0.25 μm . The coupling coefficients k_{TE} and k_{TM} are 0.04 and 0.35, respectively. For this MRR-based TM₀ polarization filter, we have $k^2\alpha^{1/2} = 3 \times 10^{-5} \ll 1.0$ for the TE mode, thus satisfying Equation (2). That is, the TE₀ is inhibited from propagating in this racetrack resonator, but the TM₀ mode can be resonant in the MRR and exit from the Drop end as output.

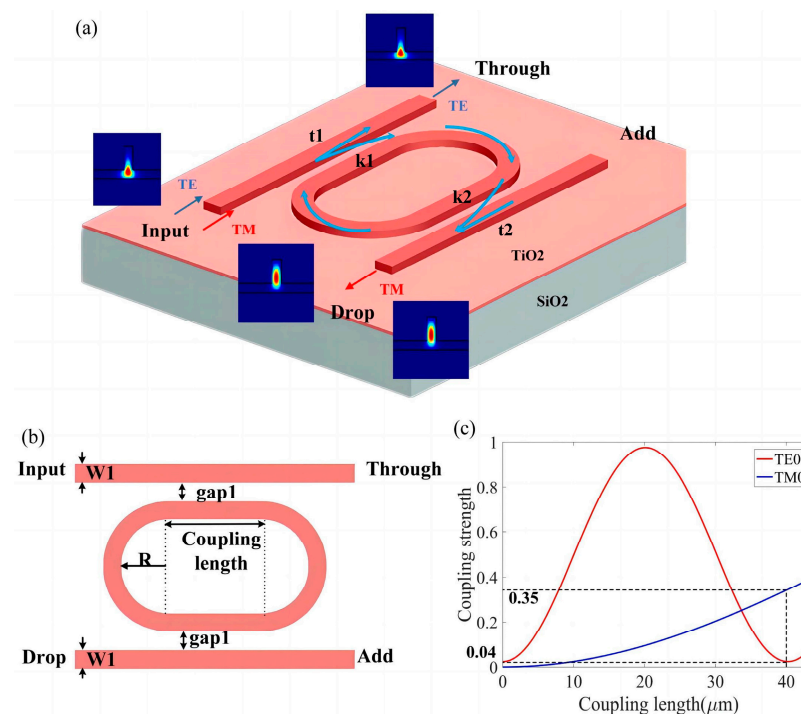


Figure 6. Schematic showing the proposed MRR-based TM polarization optical filter: (a) 3D view and (b) top view. (c) Coupling strength versus coupling length of the TE₀ and TM₀ modes, as calculated.

The spectral response of our polarization splitter was obtained using the transmission matrix method [56] and the three-dimensional finite difference time domain method. Figure 7a,b shows the transmission spectra at the Through and Drop ends when only TM and TE polarization light, respectively, of a wavelength ranging from 610 nm to 660 nm enters the waveguide. We see that there is ultra-low crosstalk between the TE₀ and TM₀ modes. Thus, according to the simulations, this MRR-based, TM-polarization-selective optical filter can realize a low loss and low crosstalk ground filtering for TM₀ input light. In contrast, the polarization extinction ratio of the TE₀ polarization mode can reach -58 dB, and resonance is suppressed, but the input TE₀ mode can easily propagate through the straight waveguide and exit from the Through end with low loss.

Due to the coupling readiness of the TE₀ mode compared with the TM₀ mode, the two fundamental polarized modes can be selectively separated by adjusting the structural parameters of the two adjacent ridge waveguides. Accordingly, we propose an r-TiO₂ MRR-based, TE-polarization-selective optical filter, as shown in Figure 8, whose coupling length and coupling distance can be tailored to inhibit coupling of the TM₀ mode and ensure complete coupling of the TE₀ mode from the straight waveguide to the racetrack waveguide.

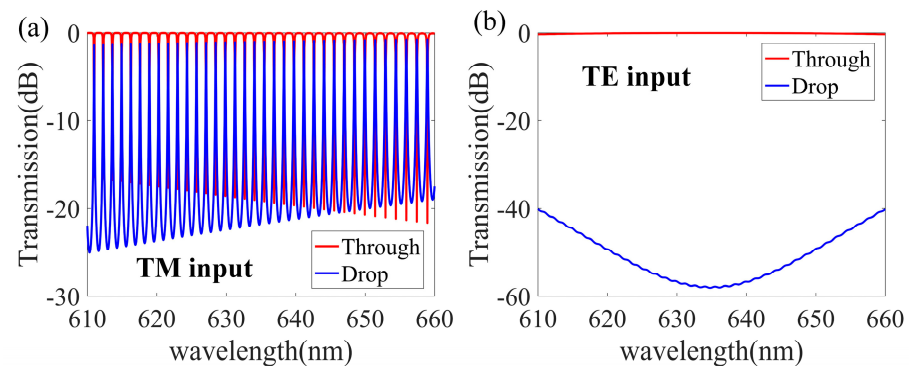


Figure 7. Simulated spectral responses for the designed TM-type polarization splitter at the Drop and Through ends when the input light is only TM polarization (a) and TE polarization (b), respectively.

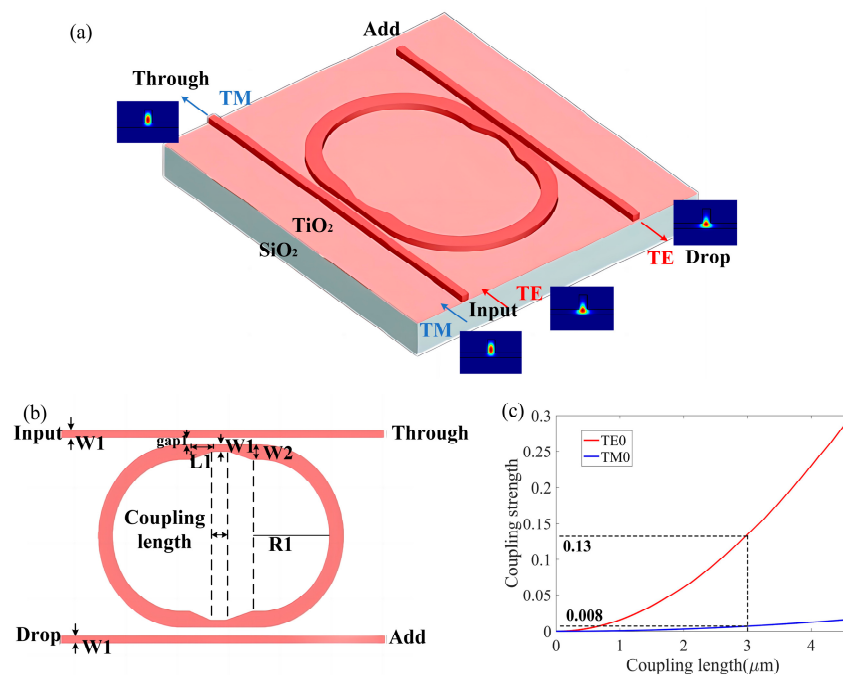


Figure 8. Schematic configuration for the MRR-based, TE-polarization-selective optical filter in a 3D view (a) and top view (b), and the calculated coupling strength of the TE₀ and TM₀ modes with different coupling lengths (c).

According to the simulation results shown in Figure 8c, if the coupling length is 3 μm and the coupling distance gap1 is 0.35 μm , the coupling coefficients are $k_{TE} = 0.13$ and $k_{TM} = 0.008$. For this MRR-based, TE-polarization-selective optical filter, the TM polarization mode has $k^2\alpha^{1/2} = 6.4 \times 10^{-5}$, which is much less than 1.0 and thus satisfies Equation (2). This means that the TM₀ mode is effectively inhibited from resonance in this polarization splitter, passing through the straight waveguide and output from the Through end with low loss. In order to reduce the bending loss in TE₀ mode in the racetrack waveguide, the dimension width W2 of the ring ridge waveguide was increased to 0.5 μm and the radius R1 was 10 μm , in which the bending radiation loss in TE₀ is less than 2 dB/cm and the cross-talking of higher modes could be negligible. To solve the width mismatch in the straight waveguide and bent waveguide in the racetrack waveguide, a tapered waveguide with a length L1 of 5 μm was added between the straight waveguide and bent waveguide, as shown in Figure 8. This designed racetrack resonator can reduce the size of the ring resonator and increase the FSR.

The spectral response of our polarization splitter is shown in Figure 9a,b for the transmission spectra of 610 nm to 660 nm light at the Through and Drop ends when

only TE and TM polarization light, respectively, are input into the waveguide. The TE polarization filter has a typical micro-ring resonance effect with low loss and low crosstalk when the input light is TE polarized. In contrast, when the input light is TM polarized, the transmittance peaks at the Drop end are as low as -40 dB, indicating TM mode resonance is effectively suppressed. With this MRR design, the TM mode can pass through the straight waveguide and exit from the Through end with low loss.

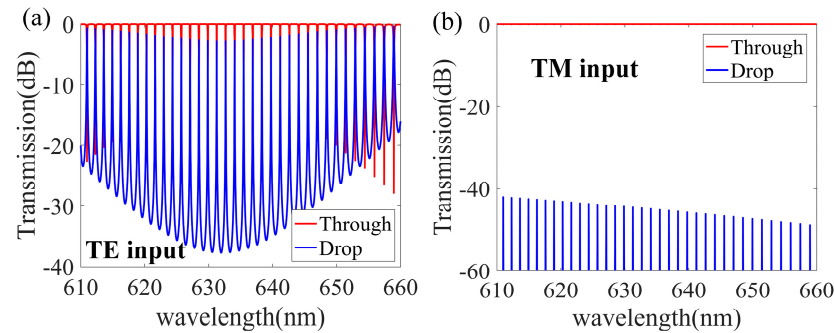


Figure 9. Simulated spectral responses in the designed TE-type polarization splitter at the Drop and Through ends when the input light is only TE polarization (a) and TM polarization (b), respectively.

A brief summary of previously reported PBSs based on different structures is presented in Table 1. It can be seen that the proposed PBS in this work is working at visible wavelengths, which is different from previous PBSs.

Table 1. Comparison of PBSs based on different structures.

Structure	Length (μm)	ER (dB)	EL (dB)	Bandwidth (nm)
LSPs [57]	1.1	20.69 (TE) 20.33 (TM)	0.249 (TE) 0.671 (TM)	(1450 nm–1650 nm) 200 nm (ER > 20 dB, TE) (ER > 12 dB, TM)
DCs [58]	11	20.32 (TE) 15.4 (TM)	1.69 (TE) 2.72 (TM)	(1530 nm–1565 nm) 35 nm (ER > 10.6 dB, TE) (ER > 14.6 dB, TM)
ADCs [59]	16	26.7 (TE) 21.3 (TM)	0.5 (TE) 0.2 (TM)	(1480 nm–1620 nm) 140 nm (ER > 10 dB, TE) (ER > 15 dB, TM)
SWGs [60]	160	25 (TE) 31 (TM)	<1	(1450 nm–1634 nm) 185 nm (ER > 20 dB, TE) (1490 nm–1575 nm) 85 nm (ER > 20 dB, TM)
ADCs [61]	31	55 (TE) 55 (TM)	0.066 (TE) 0.2 (TM)	(1500 nm–1600 nm) 100 nm (ER > 29.4 dB, TE) (1527 nm–1587 nm) 60 nm (ER > 20 dB, TM)
DCs (this work)	90	38 (TE) 43 (TM)	2 (TE) 0.45 (TM)	(610 nm–660 nm) 50 nm (ER > 40 dB, TE) (ER > 22 dB, TM)
MRRs (this work)	48	45 (TE) 58 (TM)	2.5 (TE) 0.7 (TM)	(610 nm–660 nm) 50 nm (ER > 40 dB, TE) (ER > 40 dB, TM)

4. Conclusions

In this work, a novel polarization-splitting mechanism based on the different energy distributions of the fundamental polarization modes in r-TiO₂ ridge waveguides is

proposed. The characteristics of bending loss for different bending radii and the optical coupling properties for the fundamental modes in r-TiO₂ ridge waveguide configurations are analyzed. A polarization splitter, based on DCs in the r-TiO₂ ridge waveguide structure, with a high extinction ratio for visible wavelengths, is accordingly designed. The TE₀ mode transmission at the Cross port in the TM polarization beam splitter is suppressed to as low as −40 dB, and the polarization extinction ratio of the TM₀ mode at the Through port in the TE polarization beam splitter could exceed −40 dB. In addition, polarization-selective filters based on MRRs that operate only for the resonance of TE or TM polarizations are designed. For the TM-type MRR, the transmission of the TE₀ mode at the Drop port is suppressed to only −58 dB. For the TE-type MRR, the transmission of the TM₀ mode at the Drop port is suppressed to only −40 dB. Our results suggest that a polarization splitter with a high extinction ratio working at both visible and infrared regimes in DC or MRR configurations can be achieved with simple r-TiO₂ ridge waveguide structures.

Author Contributions: Conceptualization, X.Z. and Y.M.; methodology, X.Z., Y.M. and B.X.; software, X.Z. and Y.D.; validation, X.Z., C.Z. (Chenxi Zhao) and Y.M.; formal analysis, Y.M., X.Z. and C.Z. (Chenxi Zhao); investigation, Y.M., X.Z. and C.Z. (Chenxi Zhao); resources, Y.M. and B.X.; data curation, X.Z. and C.Z. (Chenxi Zhao); writing—original draft preparation, X.Z.; writing—review and editing, Y.M. and M.Y.; visualization, X.Z. and Y.M.; supervision, Y.M., C.Z. (Cangtao Zhou) and S.R.; project administration, Y.M., J.L., F.L., C.Z. (Cangtao Zhou) and S.R.; funding acquisition, Y.M., F.X., C.Z. (Cangtao Zhou) and S.R. All authors have read and agreed to the published version of the manuscript.

Funding: This work was supported by the National Natural Science Foundation of China (Grants 12005147, 61575129, 61975094, 12105190, 62001308, 12004263, 20211062020035); the Shenzhen Science and Technology Program (Grant ZDSYS20200811143600001); the Post-Doctoral Research Project of SZTU (Grant 20180305); the Natural Science Foundation of Top Talent of SZTU (Grant 20200219); and the State Key Laboratory of Nuclear Physics and Technology, Peking University (Grant NPT2021KFJ41).

Data Availability Statement: Not applicable.

Conflicts of Interest: The authors declare no conflict of interest.

References

1. Tymon, B.; Watts, M.R. Polarization-transparent microphotonic devices in the strong confinement limit. *Nat. Photon.* **2007**, *1*, 57–60.
2. Wim, B.; Dirk, T.; Pieter, D. A polarization-diversity wavelength duplexer circuit in silicon-on-insulator photonic wires. *Opt. Exp.* **2007**, *15*, 1567–1578.
3. Hiroshi, F.; Koji, Y. Silicon photonic circuit with polarization diversity. *Opt. Exp.* **2008**, *16*, 4872–4880.
4. Dai, D.; Liu, L.; Gao, S.; Xu, D.X.; He, S. Polarization management for silicon photonic integrated circuits. *Laser Photon. Rev.* **2013**, *7*, 303–328. [[CrossRef](#)]
5. Dai, D.; Bauters, J.; Bowers, J.E. Passive technologies for future large-scale photonic integrated circuits on silicon: Polarization handling, light non-reciprocity and loss reduction. *Light Sci. Appl.* **2012**, *1*, e1. [[CrossRef](#)]
6. Dong, P.; Chen, Y.K.; Duan, G.H.; Neilson, D.T. Silicon photonic devices and integrated circuits. *Nanophotonics* **2014**, *3*, 215–228. [[CrossRef](#)]
7. Timo, P.; Ralf, P. Coherent digital polarization diversity receiver for real-time polarization-multiplexed OPSK transmission at 2.8 Gb/s. *IEEE Photon. Technol. Lett.* **2007**, *19*, 1988–1990.
8. Po, D.; Xiang, L. Monolithic silicon photonic integrated circuits for compact 100 + Gb/s coherent optical receivers and transmitters. *IEEE J. Sel. Top. Quantum Electron.* **2014**, *20*, 6100108.
9. Po, D.; Bell, L. Silicon photonic integrated circuits for wavelength-division multiplexing applications. *IEEE J. Sel. Top. Quantum Electron.* **2016**, *22*, 6100609.
10. LanTian, F.; Ming, Z. On-chip coherent conversion of photonic quantum entanglement between different degrees of freedom. *Nat. Commun.* **2016**, *7*, 11985.
11. Masa-Aki, K.; Kunimasa, S.; Masanori, K. Design of miniaturized silicon wire and slot waveguide polarization splitter based on resonant tunneling. *Opt. Exp.* **2009**, *17*, 19225–19234.
12. Lin, S.; Hu, J.; Crozier, K.B. Ultracompact, broadband slot waveguide polarization splitter. *Appl. Phys. Lett.* **2011**, *98*, 151101. [[CrossRef](#)]
13. Andrea, C.; Roberta, R.; Roberto, O. Integrated photonic quantum gates for polarization qubits. *Nat. Commun.* **2011**, *2*, 566.
14. JueMing, B.; ZhaoRong, F.; Tanumoy, P. Very-large-scale integrated quantum graph photonics. *Nat. Photon.* **2023**, *17*, 1–10.

15. Udem, T.; Holzwarth, R.; Hänsch, T.W. Optical frequency metrology. *Nature* **2002**, *416*, 233–237. [[CrossRef](#)]
16. Smullin, S.J.; Savukov, I.M.; Vasilakis, G.; Ghosh, R.K.; Romalis, M.V. Low-noise high-density alkali-metal scalar magnetometer. *Phys. Rev. A* **2009**, *80*, 033420. [[CrossRef](#)]
17. Lvovsky, A.I.; Sanders, B.C.; Tittel, W. Optical quantum memory. *Nat. Photonics* **2009**, *3*, 706–714. [[CrossRef](#)]
18. Aharonovich, I.; Englund, D.; Toth, M. Solid-state single-photon emitters. *Nat. Photonics* **2016**, *10*, 631–641. [[CrossRef](#)]
19. Aharonovich, I.; Neu, E. Diamond nanophotonics. *Adv. Opt. Mater.* **2014**, *2*, 911–928. [[CrossRef](#)]
20. Chen, Y.; Ryou, A.; Friedfeld, M.R.; Fryett, T.; Whitehead, J.; Cossairt, B.M.; Majumdar, A. Deterministic positioning of colloidal quantum dots on silicon nitride nanobeam cavities. *Nano Lett.* **2018**, *18*, 6404–6410. [[CrossRef](#)]
21. Park, Y.S.; Guo, S.; Makarov, N.S.; Klimov, V.I. Room temperature single-photon emission from individual perovskite quantum dots. *ACS Nano*. **2015**, *9*, 10386–10393. [[CrossRef](#)] [[PubMed](#)]
22. He, Y.-M.; Clark, G.; Schaibley, J.R. Single quantum emitters in monolayer semiconductors. *Nat. Nanotechnol.* **2015**, *10*, 497–502. [[CrossRef](#)] [[PubMed](#)]
23. Kern, J.; Niehues, I.; Tonndorf, P.; Schmidt, R.; Wigger, D.; Schneider, R.; Stiehm, T.; Michaelis de Vasconcellos, S.; Reiter, D.E.; Kuhn, T.; et al. Nanoscale positioning of single-photon emitters in atomically thin WSe₂. *Adv. Mater.* **2016**, *28*, 7101–7105. [[CrossRef](#)]
24. Niffenegger, R.J.; Stuart, J.; Sorace-Agaskar, C. Integrated multi-wavelength control of an ion qubit. *Nature* **2020**, *586*, 538–542. [[CrossRef](#)] [[PubMed](#)]
25. Hong, J.M.; Ryu, H.H.; Park, S.R.; Jeong, J.W.; Lee, S.G.; Lee, E.H.; Park, S.G.; Woo, D.; Kim, S.; Beom-Hoan, O. Design and fabrication of a significantly shortened multimode interference coupler for polarization splitter application. *IEEE Photon. Technol. Lett.* **2003**, *15*, 72–74. [[CrossRef](#)]
26. Jiao, Y.; Dai, D.; Shi, Y.; He, S. Shortened polarization beam splitters with two cascaded multimode interference sections. *IEEE Photon. Technol. Lett.* **2009**, *21*, 1538–1540. [[CrossRef](#)]
27. Soldano, L.B.; De Vreede, A.I.; Smit, M.K.; Verbeek, B.H.; Metaal, E.G.; Green, F.H. Mach-Zehnder interferometer polarization splitter in InGaAsP-InP. *IEEE Photon. Technol. Lett.* **1994**, *6*, 402–405. [[CrossRef](#)]
28. Dai, D.; Wang, Z.; Peters, J.; Bowers, J.E. Compact polarization beam splitter using an asymmetrical Mach-Zehnder interferometer based on silicon-on-insulator waveguides. *IEEE Photon. Technol. Lett.* **2012**, *24*, 673–675. [[CrossRef](#)]
29. Liang, T.K.; Tsang, H.K. Integrated polarization beam splitter in high index contrast silicon-on-insulator waveguides. *IEEE Photon. Technol. Lett.* **2005**, *17*, 393–395. [[CrossRef](#)]
30. Romero-García, S.; Merget, F.; Zhong, F.; Finkelstein, H.; Witzens, J. Silicon nitride CMOS-compatible platform for integrated photonics applications at visible wavelengths. *Opt. Express* **2013**, *21*, 14036–14046. [[CrossRef](#)]
31. Augustin, L.M.; Hanfoug, R. A compact integrated polarization splitter/converter in InGaAsP-InP. *IEEE Photon. Technol. Lett.* **2007**, *19*, 1286–1288. [[CrossRef](#)]
32. Shi, Y.; Dai, D.; He, S. Proposal for an ultra-compact PBS based on a photonic crystal-assisted multimode interference coupler. *IEEE Photon. Technol. Lett.* **2007**, *19*, 825–827. [[CrossRef](#)]
33. Eric, C.; Khanh, V.D.; Jean, D. Polarization beam splitting using a birefringent graded photonic crystal. *Opt. Lett.* **2013**, *38*, 459–461.
34. Tang, Y.; Dai, D.; He, S. Proposal for a grating waveguide serving as both a polarization splitter and an efficient coupler for silicon-on-insulator nanophotonic circuits. *IEEE Photon. Technol. Lett.* **2009**, *21*, 242–244. [[CrossRef](#)]
35. Ao, X.; Liu, L.; Wosinski, L.; He, S. Polarization beam splitter based on a two-dimensional photonic crystal of pillar type. *Appl. Phys. Lett.* **2006**, *89*, 171115. [[CrossRef](#)]
36. Watts, M.R.; Haus, H.A.; Ippen, E.P. Integrated mode-evolution-based polarization splitter. *Opt. Lett.* **2005**, *30*, 967–969. [[CrossRef](#)] [[PubMed](#)]
37. Winnie, Ye, N.; Xu, D.-X.; Janz, S.; Waldron, P.; Cheben, P.; Tarr, N.G. Passive broadband silicon-on-insulator polarization splitter. *Opt. Lett.* **2007**, *32*, 1492–1494.
38. Guan, X.; Wu, H.; Shi, Y.; Wosinski, L.; Dai, D. Ultracompact and broadband polarization beam splitter utilizing the evanescent coupling between a hybrid plasmonic waveguide and a silicon nanowire. *Opt. Lett.* **2013**, *38*, 3005–3008. [[CrossRef](#)]
39. Dai, D.; Bowers, J.E. Novel ultra-short and ultra-broadband polarization beam splitter based on a bent directional coupler. *Opt. Exp.* **2011**, *19*, 18614–18620. [[CrossRef](#)]
40. Zisu, G.; Rui, Y.; Wei, J. Optimal design of DC-based polarization beam splitter in lithium niobate on insulator. *Opt. Commun.* **2017**, *396*, 23–27.
41. Xu, H.; Shi, Y. On-chip silicon TE-pass polarizer based on asymmetrical directional couplers. *IEEE Photon. Technol. Lett.* **2017**, *29*, 861–864. [[CrossRef](#)]
42. Wang, X.; Fujimaki, M.; Awazu, K. Photonic crystal structures in titanium dioxide (TiO₂) and their optimal design. *Opt. Exp.* **2005**, *13*, 1486–1497. [[CrossRef](#)] [[PubMed](#)]
43. Biswajeet, G.; Jaime, C.; Michal, L. A thermal silicon microring resonators with titanium oxide cladding. *Opt. Express* **2013**, *21*, 26557–26563.
44. Djordjevic, S.S.; Shang, K.; Guan, B.; Cheung, S.T.S.; Liao, L.; Basak, J.; Liu, H.-F.; Yoo, S.J.B. CMOS-compatible, athermal silicon ring modulators clad with titanium dioxide. *Opt. Exp.* **2013**, *21*, 13958–13968. [[CrossRef](#)] [[PubMed](#)]
45. Adair, R.; Chase, L.L.; Payne, S.A. Nonlinear refractive index of optical crystals. *Phys. Rev. B* **1989**, *39*, 3337–3350. [[CrossRef](#)]

46. Long, H.; Chen, A.; Yang, G.; Li, Y.; Lu, P. Third-order optical nonlinearities in anatase and rutile TiO₂ thin films. *Thin Solid Films* **2009**, *517*, 5601–5604. [[CrossRef](#)]
47. Bernard, B.K.; Osheroff, M.R.; Hofman, A.; Mennear, J.H. Toxicology and carcinogenesis studies of dietary titanium dioxide-coated mica in male and female Fischer 344 rats. *Environ. Heal.* **1990**, *28*, 417–429. [[CrossRef](#)]
48. Ma, Y.; Zhou, C.; Xiang, B.; Yu, M.; Lu, F.; Yin, J.; Ruan, S. Fabrication of a rutile titanium dioxide thin film heterostructure using ion-implantation with Cu-Sn bonding. *Opt. Mater. Exp.* **2021**, *11*, 1196–1204. [[CrossRef](#)]
49. Huang, Q.; Yu, Y.; Yu, J. Experimental investigation on submicron rib waveguide microring/racetrack resonators in silicon-on-insulator. *Opt. Commun.* **2009**, *282*, 22–26. [[CrossRef](#)]
50. Zhu, Z.; Brown, T.G. Full-vectorial finite-difference analysis of microstructured optical fibers. *Opt. Exp.* **2002**, *10*, 853–864. [[CrossRef](#)]
51. Kane, Y. Numerical solution of initial boundary value problems involving maxwell's equations in isotropic media. *IEEE Trans. Antennas Propag.* **1966**, *14*, 302–307. [[CrossRef](#)]
52. Kedia, J.; Gupta, N. Numerical simulation of low loss silicon photonic wire waveguide with multiple cladding layers. *Opt. Quant. Electron.* **2017**, *49*, 185. [[CrossRef](#)]
53. Evans, C.C.; Liu, C.; Suntivich, J. Low-loss titanium dioxide waveguides and resonators using a dielectric lift-off fabrication process. *Opt. Express* **2015**, *23*, 11160–11169. [[CrossRef](#)]
54. Tao, S.H.; Mao, S.C.; Song, J.F.; Fang, Q.; Yu, M.B.; Lo, G.Q.; Kwong, D.L. Ultra-high order ring resonator system with sharp transmission peaks. *Opt. Exp.* **2010**, *18*, 393–400. [[CrossRef](#)]
55. Poberaj, G.; Hu, H.; Sohler, W.; Günter, P. Lithium niobate on insulator (LNOI) for micro-photonic devices. *Laser Photon. Rev.* **2012**, *6*, 488–503. [[CrossRef](#)]
56. Poon, J.K.; Scheuer, J.; Mookherjea, S.; Palocz, G.T.; Huang, Y.; Yariv, A. Matrix analysis of microring coupled resonator optical waveguides. *Opt. Express* **2004**, *12*, 90–103. [[CrossRef](#)]
57. Tan, Q.; Huang, X.; Zhou, W. A Plasmonic based Ultracompact Polarization Beam Splitter on Silicon-on-Insulator Waveguides. *Sci. Rep.* **2013**, *3*, 2206. [[CrossRef](#)]
58. Butt, M.A.; Khonina, S.N.; Kazanskiy, N.L. Compact design of a polarization beam splitter based on silicon-on-insulator platform. *Laser Phys.* **2018**, *28*, 116202. [[CrossRef](#)]
59. Zhang, L.; Fu, X.; Yang, L. Compact, Broadband and Low-Loss Polarization Beam Splitter on Lithium-Niobate-On-Insulator Using a Silicon Nanowire Assisted Waveguide. *IEEE Photonics J.* **2020**, *12*, 6601906. [[CrossRef](#)]
60. Deng, C.; Lu, M.; Sun, Y.; Huang, L.; Wang, D. Broadband and compact polarization beam splitter in LNOI hetero-anisotropic metamaterials. *Opt. Express* **2021**, *29*, 11627–11634. [[CrossRef](#)]
61. Liu, J.M.; Zhang, D.L. Compact and high-performance polarization beam splitter based on triple-waveguide coupler. *Opt. Laser Technol.* **2023**, *161*, 109159. [[CrossRef](#)]

Disclaimer/Publisher's Note: The statements, opinions and data contained in all publications are solely those of the individual author(s) and contributor(s) and not of MDPI and/or the editor(s). MDPI and/or the editor(s) disclaim responsibility for any injury to people or property resulting from any ideas, methods, instructions or products referred to in the content.